JBC RESEARCH ARTICLE

Maintaining the thyroid gland in mutant thyroglobulin–induced hypothyroidism requires thyroid cell proliferation that must continue in adulthood

Received for publication, December 13, 2021, and in revised form, May 17, 2022 Published, Papers in Press, May 23, 2022,
https://doi.org/10.1016/j.jbc.2022.102066

Xiaohan Zhang[1], Bhoomanyu Malik[1], Crystal Young[1], Hao Zhang[1], Dennis Larkin[1], Xiao-Hui Liao[2], Samuel Refetoff[2], Ming Liu[3], and Peter Arvan[1,*]

From the [1]Division of Metabolism, Endocrinology & Diabetes, University of Michigan Medical Center, Ann Arbor, Michigan, USA; [2]Departments of Medicine, Pediatrics, and Committee on Genetics, The University of Chicago, Chicago Illinois, USA; [3]Department of Endocrinology and Metabolism, Tianjin Medical University General Hospital, Tianjin, China

Edited by Ronald Wek

Congenital hypothyroidism with biallelic thyroglobulin (Tg protein, encoded by the *TG* gene) mutation is an endoplasmic reticulum (ER) storage disease. Many patients (and animal models) grow an enlarged thyroid (goiter), yet some do not. In adulthood, hypothyroid $TG^{cog/cog}$ mice (bearing a Tg-L2263P mutation) exhibit a large goiter, whereas adult WIC rats bearing the $TG^{rdw/rdw}$ mutation (Tg-G2298R) exhibit a hypoplastic thyroid. Homozygous *TG* mutation has been linked to thyroid cell death, and cytotoxicity of the Tg-G2298R protein was previously thought to explain the lack of goiter in WIC-$TG^{rdw/rdw}$ rats. However, recent studies revealed that $TG^{cog/cog}$ mice also exhibit widespread ER stress–mediated thyrocyte death, yet under continuous feedback stimulation, thyroid cells proliferate in excess of their demise. Here, to examine the relative proteotoxicity of the Tg-G2298R protein, we have used CRISPR–CRISPR-associated protein 9 technology to generate homozygous $TG^{rdw/rdw}$ knock-in mice in a strain background identical to that of $TG^{cog/cog}$ mice. $TG^{rdw/rdw}$ mice exhibit similar phenotypes of defective Tg protein folding, thyroid histological abnormalities, hypothyroidism, and growth retardation. $TG^{rdw/rdw}$ mice do not show evidence of greater ER stress response or stress-mediated cell death than $TG^{cog/cog}$ mice, and both mouse models exhibit sustained thyrocyte proliferation, with comparable goiter growth. In contrast, in WIC-$TG^{rdw/rdw}$ rats, as a function of aging, the thyrocyte proliferation rate declines precipitously. We conclude that the mutant Tg-G2298R protein is not intrinsically more proteotoxic than Tg-L2263P; rather, aging-dependent difference in maintenance of cell proliferation is the limiting factor, which accounts for the absence of goiter in adult WIC-$TG^{rdw/rdw}$ rats.

The vertebrate thyroid gland supplies the entire supply of thyroxine (also known as T_4) to the body (1). T_4 biosynthesis normally occurs upon secretion of thyroglobulin (Tg protein, encoded by the *TG* gene) (2) from thyroid epithelial cells into the (extracellular) thyroid follicle lumen, in which the secreted Tg protein is stored (3). The iodination of proteins contained within the follicle lumen (4) includes tyrosyl residues on secreted Tg (5), triggering a coupling reaction that promotes formation of T_4 within Tg (6–8). Hundreds of different *TG* gene mutations altering the primary structure of the Tg protein have been linked to defective thyroid hormone biosynthesis (9). Tg is synthesized within the endoplasmic reticulum (ER); most if not all mutant Tg is thought to misfold and become entrapped within the ER (3). As Tg is the single most abundant protein within the thyrocyte translatome, the misfolding of mutant Tg induces significant ER stress (10–15). On the one hand, primary hypothyroidism with reduced circulating thyroid hormone levels results in a compensatory upregulation of the pituitary secretion of thyroid stimulating hormone (TSH) to induce hyperplastic (*i.e.*, proliferative) thyroid gland growth (16–20); on the other hand, the ER stress caused by misfolded mutant Tg has been found to be associated with thyroid cell death in both animal models and human patients (21). Indeed, we recently demonstrated that, albeit inefficient, T_4 can be synthesized on mutant Tg released in the follicle lumen from dead thyrocytes, and thyroid goiter growth (proliferation in excess of cell death) helps to provide the cells that sustain this mechanism (21).

It is not guaranteed that net goiter growth will occur in all individuals with hypothyroidism from biallelic *TG* mutations. Whereas $TG^{cog/cog}$ (*c*ongenital *g*oiter) mice (bearing Tg-L2263P) are famous for their adult goiter (22), WIC-$TG^{rdw/rdw}$ rats (bearing Tg-G2298R) do not develop a goiter (23); this was the first model of the disease in which thyrocyte cell death was noted (24). This absence of goiter has been attributed to increased *rdw-Tg* proteotoxicity (25). However, original descriptions of the thyroid phenotype of $TG^{cog/cog}$ mice and WIC-$TG^{rdw/rdw}$ rats were limited to the very different AKR/J mouse and Wistar–Imamichi rat strain backgrounds, respectively, in which species- and strain-specific genetic interactions might distinctly alter the balance of thyroid cell growth and death. JAX laboratories currently distribute the TG^{cog} allele in the C57BL6J background, and here, we have used CRISPR/CRISPR-associated protein 9 (Cas9) technology to generate homozygous $TG^{rdw/rdw}$ knock-in mice in the same strain

* For correspondence: Peter Arvan, parvan@umich.edu.

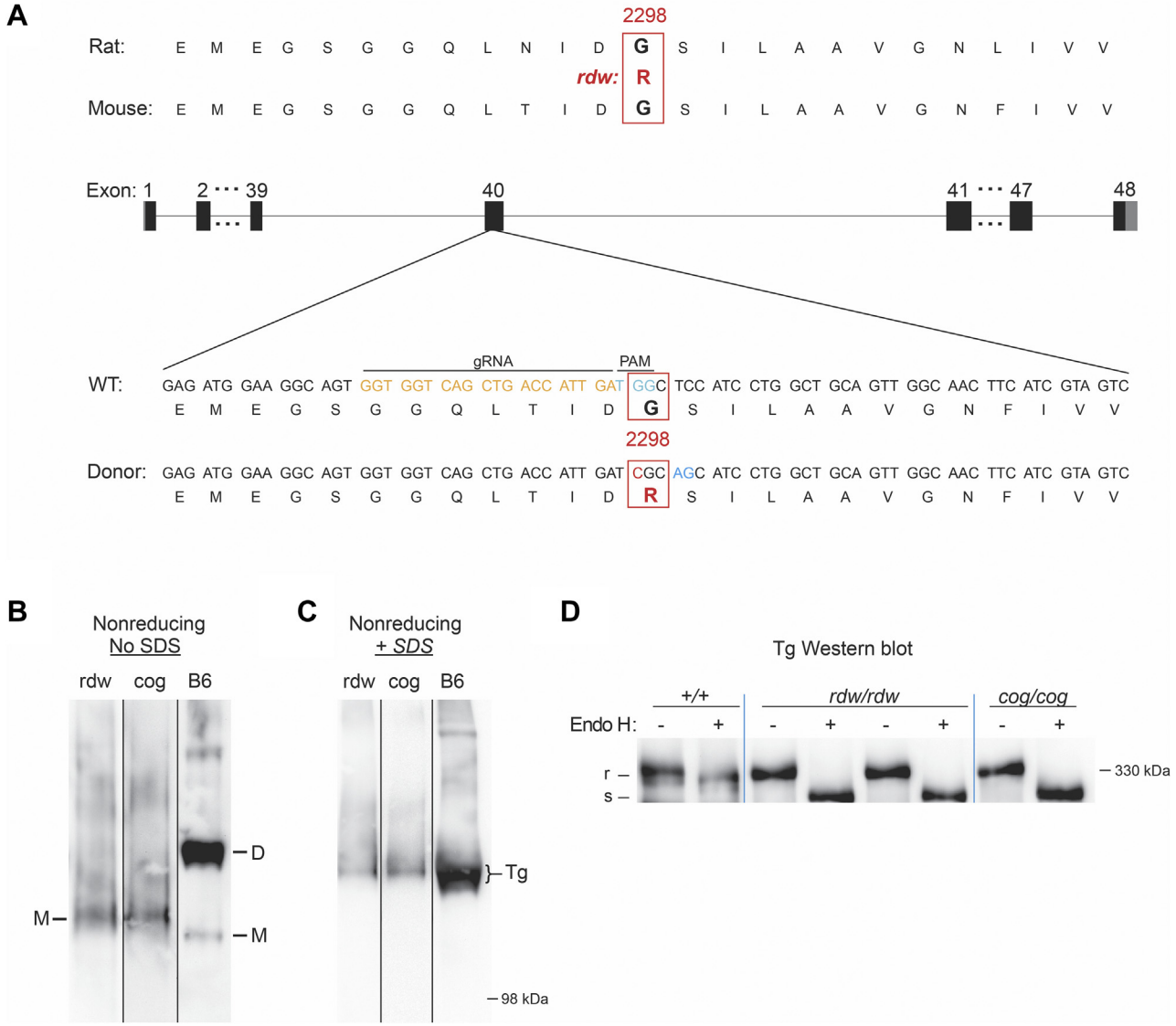

Figure 1. Generation of $TG^{rdw/rdw}$ mice. *A*, schematic illustration of CRISPR/Cas9-mediated gene editing to knock-in *rdw* (Tg-G2298R) mutation within the exon 40 of the mouse *TG* gene. The target Tg protein sequences and the target site of gRNA are indicated. *B* and *C*, polyacrylamide gel electrophoresis of thyroid homogenates from B6, $TG^{rdw/rdw}$, and $TG^{cog/cog}$ mice in the absence (*B*) or the presence (*C*) of SDS, followed by immunoblotting with an mAb anti-Tg (three repeats). *D*, endoglycosidase H digest and Tg Western blotting of thyroid from B6, $TG^{rdw/rdw}$, and $TG^{cog/cog}$ mice (n = 3 animals per group). Cas9, CRISPR-associated protein 9; gRNA, guide RNA; mAb, monoclonal antibody; *TG*, thyroglobulin gene; Tg, thyroglobulin protein.

background. Our analysis indicates that the gene product of the TG^{rdw} allele is not intrinsically more proteotoxic than that of the TG^{cog} allele, and our data suggest an alternative explanation for the incapacity of WIC-$TG^{rdw/rdw}$ rats to maintain their hypothyroid goiter in adulthood.

Results

Generation of $TG^{rdw/rdw}$ *mice*

Using CRISPR/Cas9 with a suitable guide RNA, we introduced within C57BL6J mouse *TG* exon 40, the point mutation that encodes Tg-G2298R (Fig. 1*A*; in the UniProt P01266 system, this numbering would need to add 19 to account for the signal peptide), just 35 residues from the site of the *cog* mutation in the ChEL domain of Tg (Fig. S1). After crossing with C57BL6J, animals were bred to homozygosity so that $TG^{rdw/rdw}$ mice could be compared with $TG^{cog/cog}$ mice in the identical genetic background. Resection of the thyroid gland of adult animals was followed by tissue homogenization in buffer lacking all denaturants, followed by nondenaturing polyacrylamide gel electrophoresis (*i.e.*, in the absence of SDS, mobility is dependent not on protein mass but rather on charge/mass ratio and hydrodynamic radius (26), and this has been used to separate unfolded and folded Tg monomers from native Tg dimers (27, 28)). After electrotransfer to nitrocellulose and immunoblotting with anti-Tg antibody, immunoreactive Tg in WT-control C57BL6J thyroids appeared primarily as two bands corresponding to folded Tg monomers (a smaller quantity) and dimers (a larger quantity, Fig. 1*B* marked "M" and "D"). However, mutant Tg protein from $TG^{cog/cog}$ and $TG^{rdw/rdw}$ mouse thyroids both appeared primarily as a monomer of slower electrophoretic mobility

(Fig. 1*B*) indicating a less compact structure consistent with an unfolded state (28). When the same samples were analyzed under denaturing conditions by nonreducing SDS-PAGE—although the molecular masses of cog-Tg-L2263P, rdw-Tg-G2298R, and WT-Tg are identical—the mobility of WT-Tg still appeared slightly faster (Fig. 1*C*), suggesting a more tightly disulfide-linked structure (29, 30). Moreover, in WT thyroid glands, nearly all Tg proteins had migrated out of the ER so that most glycans on those Tg molecules were processed to complex sugars resistant to digestion with endoglycosidase H (Fig. 1*D*, marked as "R"), whereas all Tg proteins in $TG^{cog/cog}$ and $TG^{rdw/rdw}$ mouse thyroids remained fully endoglycosidase H-sensitive (Fig. 1*D*, "S"), indicating failure of the mutant Tg protein to arrive at the Golgi complex.

Thyroid histology of $TG^{rdw/rdw}$ *mice*

Careful examination of the histology of $TG^{rdw/rdw}$ and $TG^{cog/cog}$ mouse thyroid glands revealed important differences with that of the WT thyroid. While all three tissues exhibited prominent eosinophilic staining consistent with accumulation of Tg protein, in WT ($TG^{+/+}$) thyroid, the Tg protein was primarily localized extracellularly in the follicle lumen, whereas in $TG^{rdw/rdw}$ and $TG^{cog/cog}$ mouse thyroid glands, most Tg proteins were found in an expanded and a distorted cytoplasm within the thyrocytes (Fig. 2*A*), although there was some aberrant material in the follicle lumen (that we have recently established is comprised of the detritus of dead cells (21)). From multiple images of thyroid sections derived from 3-month-old animals of each genotype, the cross-sectional area of individual thyrocytes was abnormally expanded approximately eightfold in $TG^{rdw/rdw}$ and $TG^{cog/cog}$ mouse thyroid glands (Fig. S2*A*) with a fraction of total cellular area occupied by cytoplasm increased to >90% (Fig. S2*B*) plus an increase of cross-sectional nuclear area (Fig. S2*C*). With the huge expansion of cytoplasm, the number of thyrocytes actually accommodated within each follicle profile shrank nearly in half (Fig. S2*D*).

To independently confirm whether Tg protein in mouse thyroid glands was primarily extracellular or intracellular, we coimmunostained these tissues for Tg and ezrin, which delimits the follicle lumen at the apical plasma membrane of thyrocytes. Whereas Tg in WT glands was contained within the ezrin ring (*i.e.*, extracellular, in the follicle lumen), the

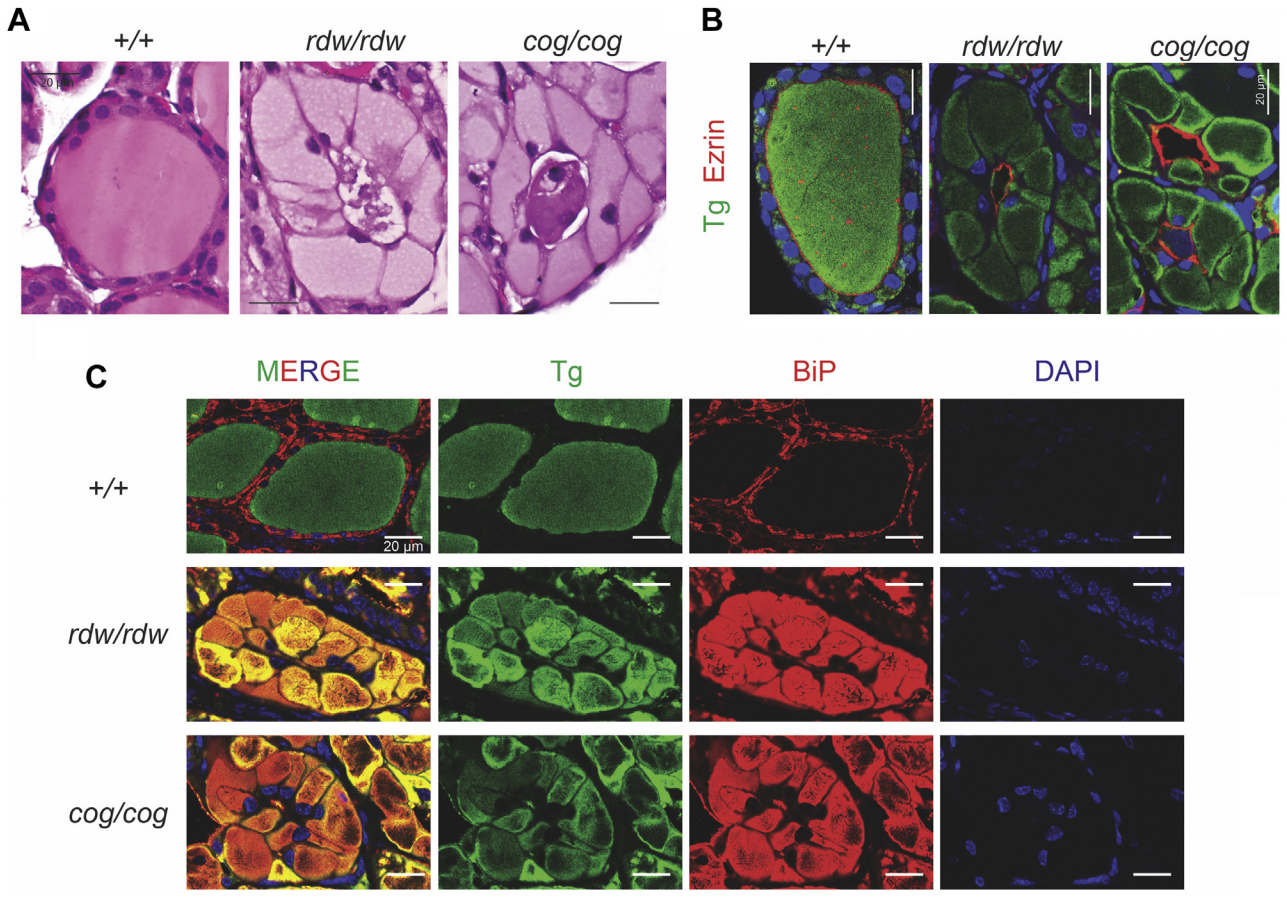

Figure 2. Thyroid histology of $TG^{rdw/rdw}$ mice. *A*, representative H&E of thyroid glands from B6, $TG^{rdw/rdw}$, and $TG^{cog/cog}$ mice (n = 5–8 animals per group), showing thyrocyte distention in $TG^{rdw/rdw}$ and $TG^{cog/cog}$ mice. The scale bars represent 20 μm. *B*, immunofluorescence of anti-Tg (*green*) and antiezrin (*red*) of thyroid glands from B6, $TG^{rdw/rdw}$, and $TG^{cog/cog}$ mice (n = 5 animals per group), with DAPI counterstaining (*blue*). The scale bars represent 20 μm. *C*, immunofluorescence of Tg (*green*) and anti-BiP (*red*) of thyroid glands from B6, $TG^{rdw/rdw}$, and $TG^{cog/cog}$ mice (n = 5 animals per group), with DAPI counterstaining (*blue*). The scale bars represent 20 μm. BiP, immunoglobulin heavy-chain binding protein; DAPI, 4′,6-diamidino-2-phenylindole; *TG*, thyroglobulin gene; Tg, thyroglobulin protein.

mutant Tg protein in $TG^{rdw/rdw}$ and $TG^{cog/cog}$ mice was largely excluded from within the ezrin ring, indicating that it had not been transported from thyrocytes to the follicle lumen (Figs. 2*B* and S3). Indeed, in WT ($TG^{+/+}$) thyroid, the Tg protein distribution was largely nonoverlapping with the ER molecular chaperone, BiP (immunoglobulin heavy-chain binding protein); whereas in $TG^{rdw/rdw}$ and $TG^{cog/cog}$ mouse thyroid glands, the Tg protein was essentially exclusively contained within the swollen ER, colocalized with BiP (Fig. 2*C*).

Hypothyroidism of $TG^{rdw/rdw}$ *mice*

As $TG^{cog/cog}$ mice have goiter from hypothyroidism (31), we wished to determine if $TG^{rdw/rdw}$ mice were even more hypothyroid by comparing them to $TG^{cog/cog}$ mice at 3 months of age and again at 11 months. At 3 months, both sets of mutant animals had >75% inhibition of circulating total T_4 and >65% inhibition of circulating total triiodothyronine (T_3), accompanied by dramatic elevation of murine TSH that averaged ~25,000 mU/l (Fig. 3*A*). Accompanying the thyroid hormone defect was body growth retardation for both sets of mutant animals (Fig. 3*B*), which has been reported in other models of congenital hypothyroidism (32).

In both $TG^{rdw/rdw}$ and $TG^{cog/cog}$ mice, the highly elevated TSH levels tended to decline by more than 50% by 11 months (Fig. 3), either as an aging-related phenomenon or possibly consistent with a small improvement in thyroid hormone output by the mutant thyroid glands over time (which, in the case of $TG^{cog/cog}$ mice, is known to be accompanied by goiter growth (22)). Notably, when compared with $TG^{cog/cog}$ mice, $TG^{rdw/rdw}$ mice never had more elevated TSH (or diminished T_4 or T_3) levels or more severe growth retardation, indicating that $TG^{rdw/rdw}$ mice did not have more severe hypothyroidism than $TG^{cog/cog}$ mice at any age examined (Fig. 3).

Chronic ER stress in the thyroid glands of $TG^{rdw/rdw}$ *mice*

In the thyroid gland at 3 months of age, $TG^{rdw/rdw}$ mice showed elevated levels of BiP (normalized to tubulin as a loading control), as was also the case in $TG^{cog/cog}$ mice (Fig. 4*A*)—indicative of ongoing ER stress. In addition, the BiP cochaperone $p58^{ipk}$ was also clearly elevated in the mutant thyroid glands compared with WT (Fig. 4*A*). The ratio of phosphorylated eukaryotic initiation factor 2α (phospho-eIF2α) to total eIF2α, suggestive of activation of the ER stress sensor, PERK—was elevated in the thyroid glands of both

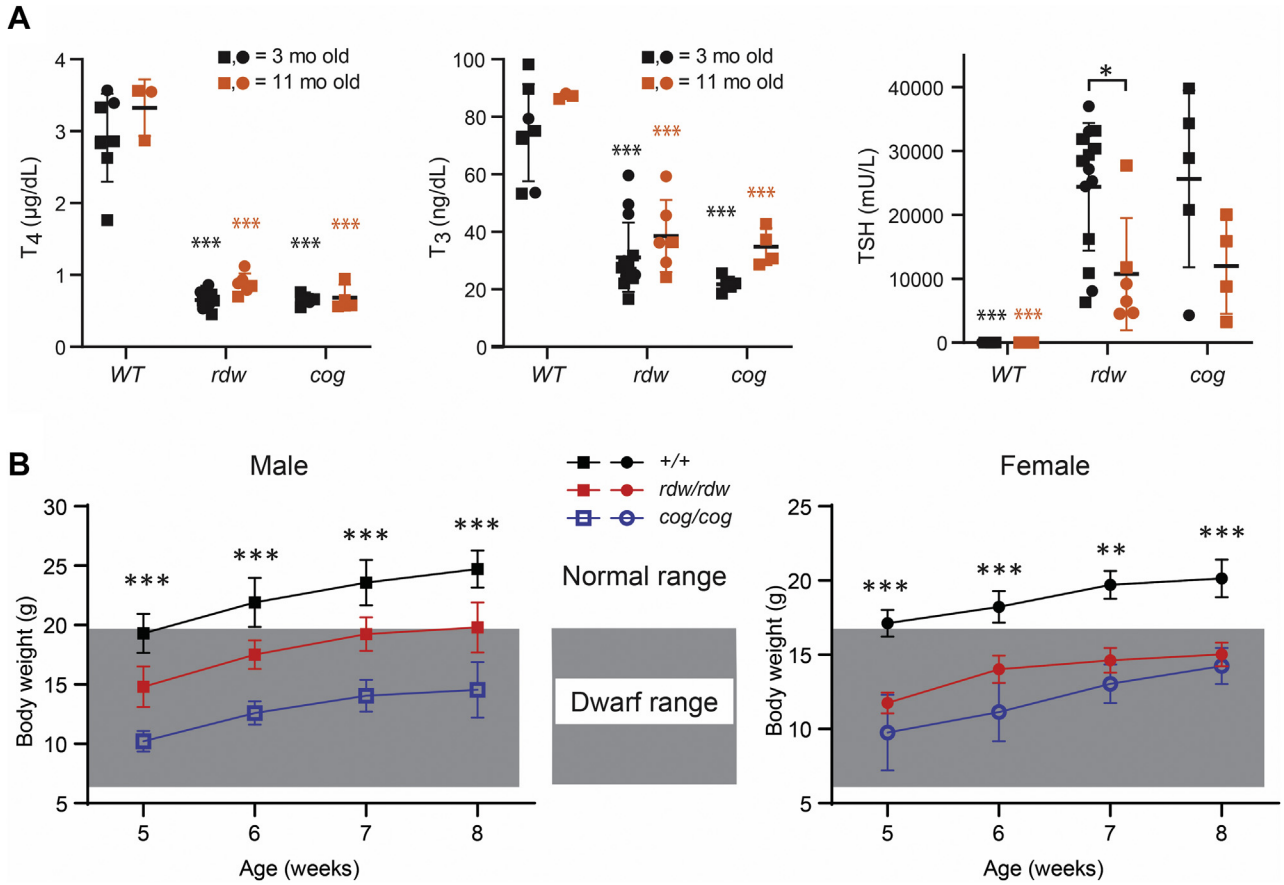

Figure 3. Hypothyroidism of $TG^{rdw/rdw}$ **mice.** *A*, serum total T_4, T_3, and TSH levels of B6, $TG^{rdw/rdw}$, and $TG^{cog/cog}$ mice at 3 months (*black*) and 11 months (*red*) of age (males shown as *squares* and females as *circles*). Data are mean ± SD; *$p < 0.05$, #$p < 0.001$ compared with B6 mice of 3 months old, &$p < 0.001$ compared with B6 mice of 11 months old. *B*, body weight of B6 (*black*), $TG^{rdw/rdw}$, (*red*) and $TG^{cog/cog}$ mice (*blue*). The *shaded area* indicates the body weights of dwarf mice. Data are mean ± SD; **$p < 0.01$, ***$p < 0.001$ compared with B6 mice. T_3, triiodothyronine; T_4, thyroxine; *TG*, thyroglobulin gene; TSH, thyroid stimulating hormone.

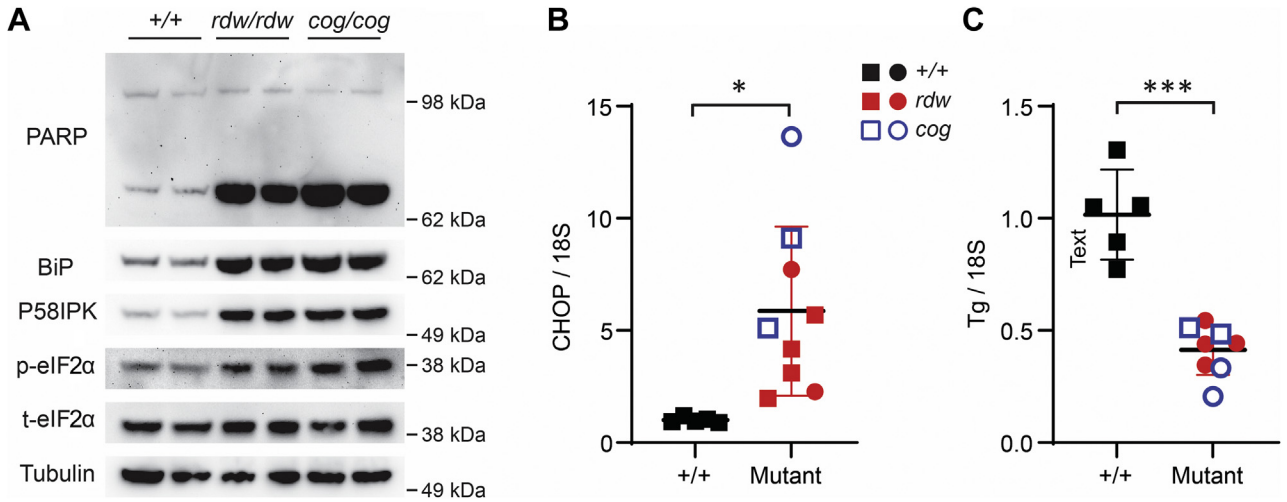

Figure 4. Chronic ER stress in the thyroid glands of $TG^{rdw/rdw}$ mice. *A*, BiP, p58ipk, phospho-eIF2α, and PARP (by Western blotting) in the thyroid glands of B6, $TG^{rdw/rdw}$, and $TG^{cog/cog}$ mice (n = 3 animals per group, two of which are shown in the panel). *B*, CHOP mRNA levels (normalized to 18S) in the thyroid glands of B6, $TG^{rdw/rdw}$ (*purple*), and $TG^{cog/cog}$ (*orange*) mice (n = 3–6 animals per group; each point represents a single animal; *square* = male, *circle* = female). Data are shown as mean ± SD; $*p < 0.05$. *C*, Tg mRNA levels (normalized to 18S) in the thyroid glands of B6 (*black symbols*), $TG^{rdw/rdw}$ (*red symbols*), and $TG^{cog/cog}$ (*blue symbols*) mice (n = 4–5 animals per group; each point represents a single animal; *square* = male, *circle* = female). Data are shown as mean ± SD; $***p < 0.001$. BiP, immunoglobulin heavy-chain binding protein; CHOP, CCAAT/enhancer-binding protein homologous protein; eIF2α, eukaryotic initiation factor 2α; ER, endoplasmic reticulum; PARP, poly(ADP-ribose) polymerase; *TG*, thyroglobulin gene; Tg, thyroglobulin protein.

mouse mutants. Importantly, none of these ER stress markers were more elevated in the thyroid glands of $TG^{rdw/rdw}$ mice than in $TG^{cog/cog}$ mice (Fig. 4*A*). Compared with WT mice, elevation of CCAAT/enhancer-binding protein homologous protein (CHOP) mRNA level in the thyroid gland was increased in both $TG^{rdw/rdw}$ mice and $TG^{cog/cog}$ mice (Fig. 4*B*) but again was not more elevated in $TG^{rdw/rdw}$ mice (4.1 ± 2.2 fold) than in $TG^{cog/cog}$ mice (13.2 ± 8.7 fold). Moreover, because chronic continuous ER stress has been associated with subtle signs of dedifferentiation in thyrocytes (11, 33) as well as Ire1-mediated mRNA decay (in various cell types (34–36)), we examined thyroidal *TG* mRNA levels and observed an average decrease of 56 ± 8% of WT levels in $TG^{rdw/rdw}$ mice and 62 ± 14% in $TG^{cog/cog}$ mice—both significantly different from WT but not different from each other (Fig. 4*C*). Finally, in conjunction with the chronically increased ER stress, cell death signaling as measured by poly(ADP-ribose) polymerase (PARP) cleavage was apparent in the thyroid glands of both mutant animals—but with no evidence of greater PARP cleavage in $TG^{rdw/rdw}$ mice than in $TG^{cog/cog}$ mice (Fig. 4*A*).

Because both $TG^{cog/cog}$ mice and WIC-$TG^{rdw/rdw}$ rats are known to exhibit intrathyroidal cell death (21), we performed TUNEL staining on the newly engineered $TG^{rdw/rdw}$ mice. As expected, the thyroid glands of $TG^{rdw/rdw}$ mice revealed 4′,6-diamidino-2-phenylindole (DAPI; Invitrogen)–positive nuclear material within the lumen of thyroid follicles, associated with positive TUNEL staining (Fig. 5*A*). While thyrocyte cell death in the mutant mice was significantly greater than background TUNEL staining seen in WT mouse thyroid glands, the $TG^{rdw/rdw}$ mice did not exhibit greater TUNEL staining than that found in $TG^{cog/cog}$ thyroid (Fig. 5*B*). Altogether from the results of Figs. 4 and 5, although homozygous expression of Tg-G2298R does indeed produce hypothyroidism, we found no evidence to suggest that this mutant Tg yields more ER stress or more proteotoxicity than the Tg-L2263P expressed in $TG^{cog/cog}$ mice.

Thyroid cell proliferation during chronic ER stress in the thyroid glands of animals bearing TG mutations

We recently reported that in WIC rats, $TG^{rdw/rdw}$ homozygotes do begin to develop thyroid enlargement within the first two postnatal months, but their absence of goiter in adulthood involves an inability to maintain the goiter as a function of aging (21). As $TG^{cog/cog}$ mice exhibit thyroid cell death (Fig. 5) but nevertheless manage to grow a large goiter in adulthood, we turned attention to thyroid cell proliferation. By Ki-67 immunostaining of mouse thyroid glands, it was apparent that both $TG^{rdw/rdw}$ and $TG^{cog/cog}$ mutants exhibited sustained enhancement of thyroid cell proliferation well into adulthood (11 months, Fig. 6*A*). When quantified, $TG^{rdw/rdw}$ mice, on average, definitely did not exhibit less thyroid cell proliferation than that observed in $TG^{cog/cog}$ mice—and both exhibited significantly greater proliferation than that found in the thyroids of WT animals (Fig. 6*B*). As ER stress–mediated cell death was not increased (Figs. 4 and 5) and thyroid cell proliferation was not diminished (Fig. 6*B*), there was no reason why $TG^{rdw/rdw}$ mice would not grow a goiter as large as that found in $TG^{cog/cog}$ mice. Indeed, when allowed to survive over the first postnatal year of life, multinodular goiters in $TG^{rdw/rdw}$ mice at least as large as those found in $TG^{cog/cog}$ mice appeared (Fig. S4); vastly larger than the thyroid glands seen in WT animals (Fig. 6*C*).

Because WIC-$TG^{rdw/rdw}$ rats have a dramatic loss of thyroid tissue mass during adulthood (21), the goitrogenesis in $TG^{rdw/rdw}$ mice seemed perplexing. We therefore returned to WIC-$TG^{rdw/rdw}$ rats to examine thyroid cell proliferation as a function of postnatal age. As noted previously, it is established

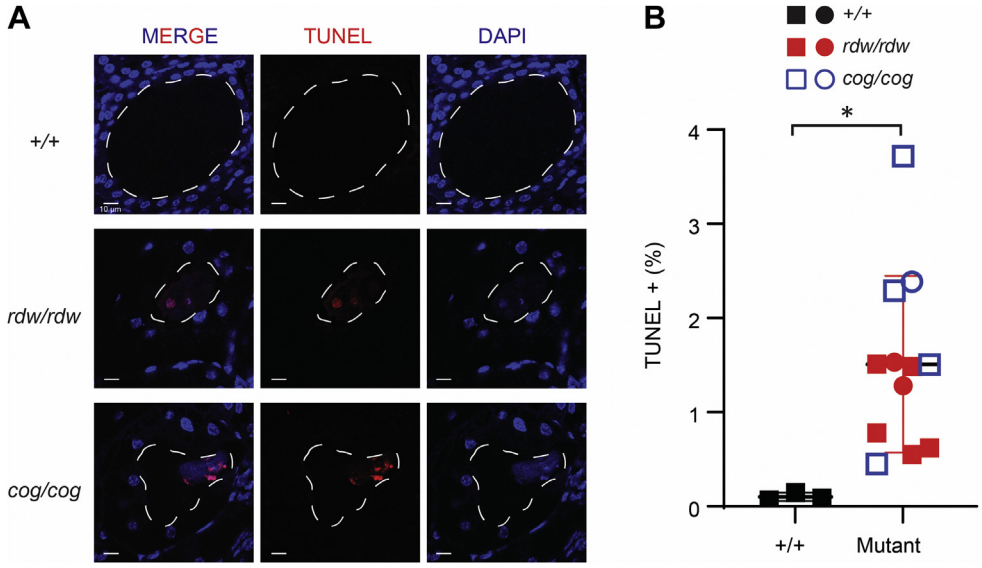

Figure 5. Thyroid cell death in $TG^{rdw/rdw}$ mice. *A*, representative TUNEL labeling (*red*) with DAPI counterstain (*blue*) in the thyroid sections of B6, $TG^{rdw/rdw}$, and $TG^{cog/cog}$ mice (n = 3–7 animals per group). A *dashed white line* delimits the thyroid follicle lumen. The scale bars represent 10 μm. *B*, quantification of *A* presented as TUNEL-positive nuclei in the proportion of total nuclei in the thyroids of B6 (*black symbols*), $TG^{rdw/rdw}$ (*red symbols*), and $TG^{cog/cog}$ (*blue symbols*) mice (n = 3–7 animals per group; each point represents a single animal; *square* = male, *circle* = female). Data are mean ± SD; *$p < 0.05$. DAPI, 4′,6-diamidino-2-phenylindole; *TG*, thyroglobulin gene.

that WIC-$TG^{rdw/rdw}$ rats do exhibit exuberant thyroid gland growth during the first two postnatal months of life (21); indeed, at 8 weeks of age, there was a dramatic increase of thyroidal Ki-67 immunostaining (Fig. 7, *A* and *B*). To our surprise, however, unlike in $TG^{rdw/rdw}$ mice (in the C57BL6J genetic background, Fig. 6, *A* and *B*), by early adulthood, the hypothyroid WIC-$TG^{rdw/rdw}$ rats no longer exhibited thyroid cell proliferation beyond control levels, and this feature persisted as the animals aged further (Fig. 7, *A* and *B*). It has been repeatedly reported that WIC-$TG^{rdw/rdw}$ rats during this period of life (18–40 weeks) do maintain markedly elevated circulating TSH levels (23, 37–39), and indeed, we found that older WIC-$TG^{rdw/rdw}$ rats (>30 weeks) exhibited a circulating TSH (32.7 ± 10.7 ng/ml; n = 10) that was 16.6-fold elevated over that of their WT counterparts (1.97 ± 0.11 ng/ml; n = 3). To confirm that the elevated TSH in adult WIC rats should be sufficiently bioactive to stimulate thyroid cell proliferation, we challenged 14-week-old WT WIC rats to induce hypothyroidism, by introducing propylthiouracil (PTU) continuously for 3 weeks before euthanasia and thyroid tissue analysis at 17 weeks. This treatment yielded a similar elevation of circulating TSH (35.8 ± 1.01 ng/ml; n = 3), and these older hypothyroid WT WIC rats exhibited exuberant thyroid cell proliferation well beyond control levels (Fig. 8, *A* and *B*). The data suggest that the WIC strain background is specifically deficient neither for a central nervous system response to hypothyroidism nor for the bioactivity of TSH in older animals. Thus, we conclude that the inability of WIC-$TG^{rdw/rdw}$ rats to expand thyroidal mass in adulthood is caused neither by a genetic deficiency of the central nervous system axis to provide adequate feedback stimulation nor solely by ER stress–mediated thyroid cell death, but rather by an inability of the adult WIC-$TG^{rdw/rdw}$ rat strain to maintain the TSH-driven thyroid cell proliferative response to hypothyroidism that is needed for net thyroid gland growth.

Discussion

Chronic, unremitting, and unresolved ER stress is a factor that can promote cell death (40); thus, the field of medicine is just beginning to attack ER stress–mediated cell death as a potential therapeutic approach to address various clinical disorders (41, 42). However, from studies of hypothyroid patients and animal models bearing biallelic *TG* mutations (10) as well as cell culture models of the disease (43), we have been mostly impressed by continued thyrocyte proliferation (11) despite the ongoing stress-mediated thyrocyte cell death (21). In such a case, the entire thyroid gland overgrows, that is, beyond normal size (22). Nevertheless, in individuals with hypothyroidism from biallelic *TG* mutations, net thyroid growth is not always observed. This is also the case in WIC-$TG^{rdw/rdw}$ rats, which initiate thyroid growth during the first one or two postnatal months (21) but in adulthood lose the ability to further expand or even maintain the goiter, leading ultimately to thyroid atrophy (23). Despite the remarkably close physical proximity of the encoded mutation from that seen in $TG^{cog/cog}$ mice (Fig. S1), we considered the possibility that the TG^{rdw}-encoded Tg-G2298R protein might be intrinsically more proteotoxic than the TG^{cog}-encoded Tg-L2263P protein. Such a hypothesis can only be tested by comparing the cell biological and physiological impact of the two mutant proteins in the identical genetic background. This was made possible using CRISPR/Cas9 technology to engineer the TG^{rdw} allele into C57BL6J mice (Fig. 1*A*).

From our analysis, it was immediately apparent that $TG^{rdw/rdw}$ mice did not exhibit greater misfolding of the

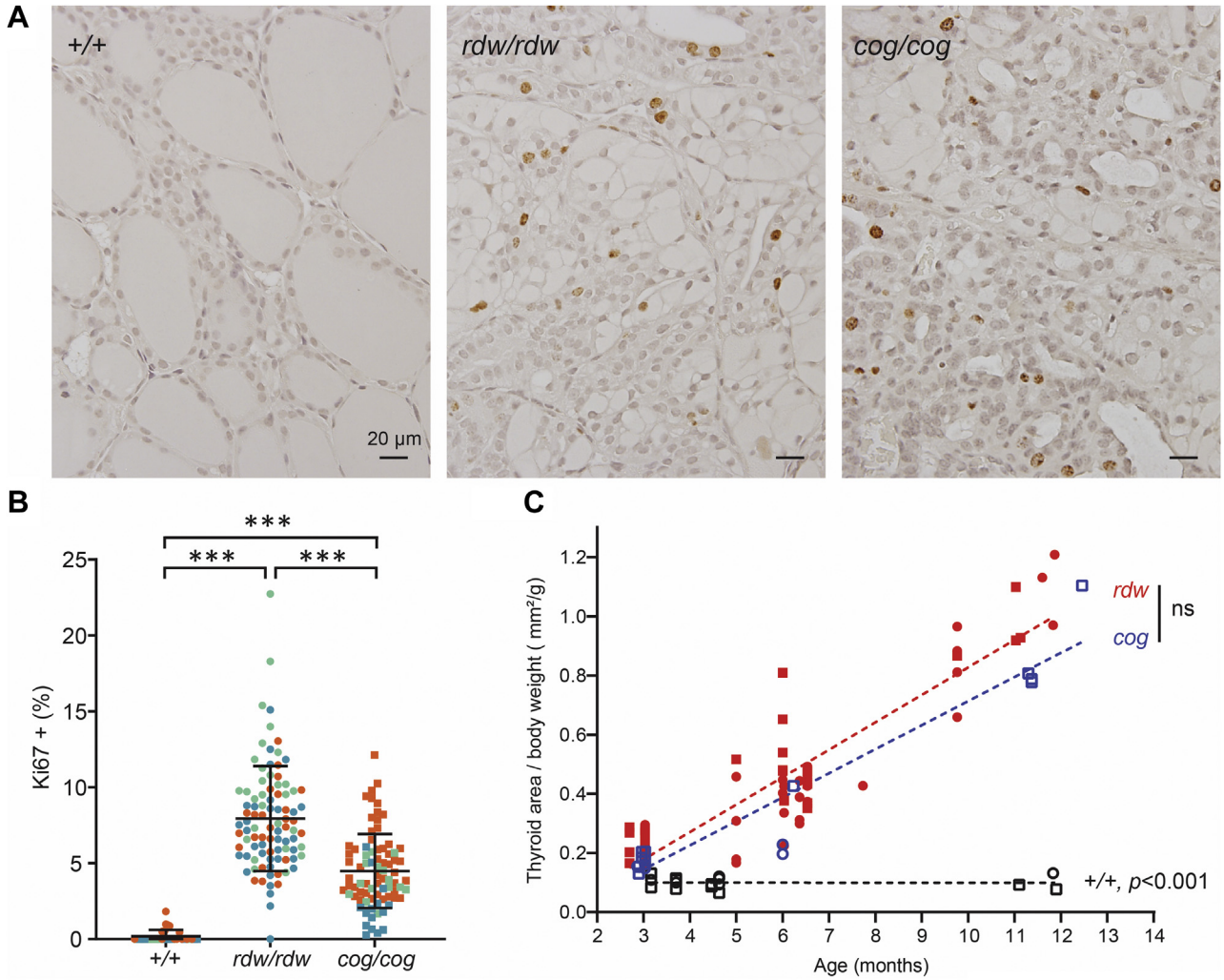

Figure 6. Thyroid cell proliferation in $TG^{rdw/rdw}$ mice. *A*, Ki67 immunohistochemistry of the thyroid gland of WT, $TG^{rdw/rdw}$, and $TG^{cog/cog}$ mice (11 months). There are sustained thyroid cell proliferation in both $TG^{rdw/rdw}$ and $TG^{cog/cog}$ mice. The scale bars represent 20 μm. *B*, quantification of images like those shown in *A*, presented as Ki67-positive nuclei as a proportion of total nuclei in thyroid images from 11-month-old WT, $TG^{rdw/rdw}$, and $TG^{cog/cog}$ mice (n = 3 animals per group; each color represents a single animal; each point is an independent section; *square* = male, *circle* = female). Data are mean ± SD; ***$p <$ 0.001. *C*, thyroid gland size (normalized to body weight) as a function of age (*square* = male, *circle* = female). A *dashed line* shows the linear regression of the thyroid size in WT, $TG^{rdw/rdw}$, and $TG^{cog/cog}$ mice. No significance difference was observed between thyroid glands of $TG^{rdw/rdw}$ and $TG^{cog/cog}$ mice. *TG*, thyroglobulin gene.

mutant Tg protein (Fig. 1, *B* and *C*) or greater failure of Tg export from the ER to that seen in $TG^{cog/cog}$ mice (Fig. 1*D*). In addition, the ER entrapment of mutant Tg led to enormous ER swelling that was comparable in the two mouse models (Fig. 2). Furthermore, $TG^{rdw/rdw}$ mice exhibited profound primary hypothyroidism with body growth retardation and initial elevation of circulating TSH level to ∼25,000 mU/l, which was not greater than that in $TG^{cog/cog}$ mice (Fig. 3). Unlike what has been reported in the original AKR/J mouse strain (22), neither $TG^{rdw/rdw}$ nor $TG^{cog/cog}$ mice in the C57BL6/J background (from JAX laboratories; fed Formulab Diet 5008 bearing 0.8–0.97 ppm iodine) could spontaneously restore circulating T_4 to euthyroid levels by 11 months of age; instead showing only marginal improvement of their dramatically elevated levels of circulating TSH (Fig. 3*A*). Furthermore, although $TG^{rdw/rdw}$ mice exhibited a major increase of thyroidal ER stress markers and ER stress–mediated cell death, it was not worse than in $TG^{cog/cog}$ mice (Figs. 4 and 5), consistent with the notion that in both cases, endogenous thyroid hormone synthesis derived from dead thyrocytes (21) is a highly inefficient process compared with the normal hormonogenesis process occurring in WT thyroid glands. Yet despite the cell death, hypothyroid $TG^{rdw/rdw}$ mice exhibited exuberant thyroid cell proliferation (Fig. 6*A*), which was not less than that in $TG^{cog/cog}$ mice (Fig. 6*B*). Indeed, it is this feature that led ultimately to goiters in $TG^{rdw/rdw}$ mice that were not smaller than those observed in $TG^{cog/cog}$ mice (Fig. 6*C*). Taken together, the primary conclusion of this work is that when compared side by side in the same strain background, there is no greater thyroidal proteotoxicity caused by the mutant Tg-G2298R than by Tg-L2263P.

It is the failure to sustain thyroid cell proliferation in adult WIC-$TG^{rdw/rdw}$ rats (Fig. 7) that leads to the loss of thyroid tissue mass in these animals (21). What could be the cause of this failure to maintain cell proliferation in WIC-$TG^{rdw/rdw}$ rats? We considered the possibility that either the extent of rat

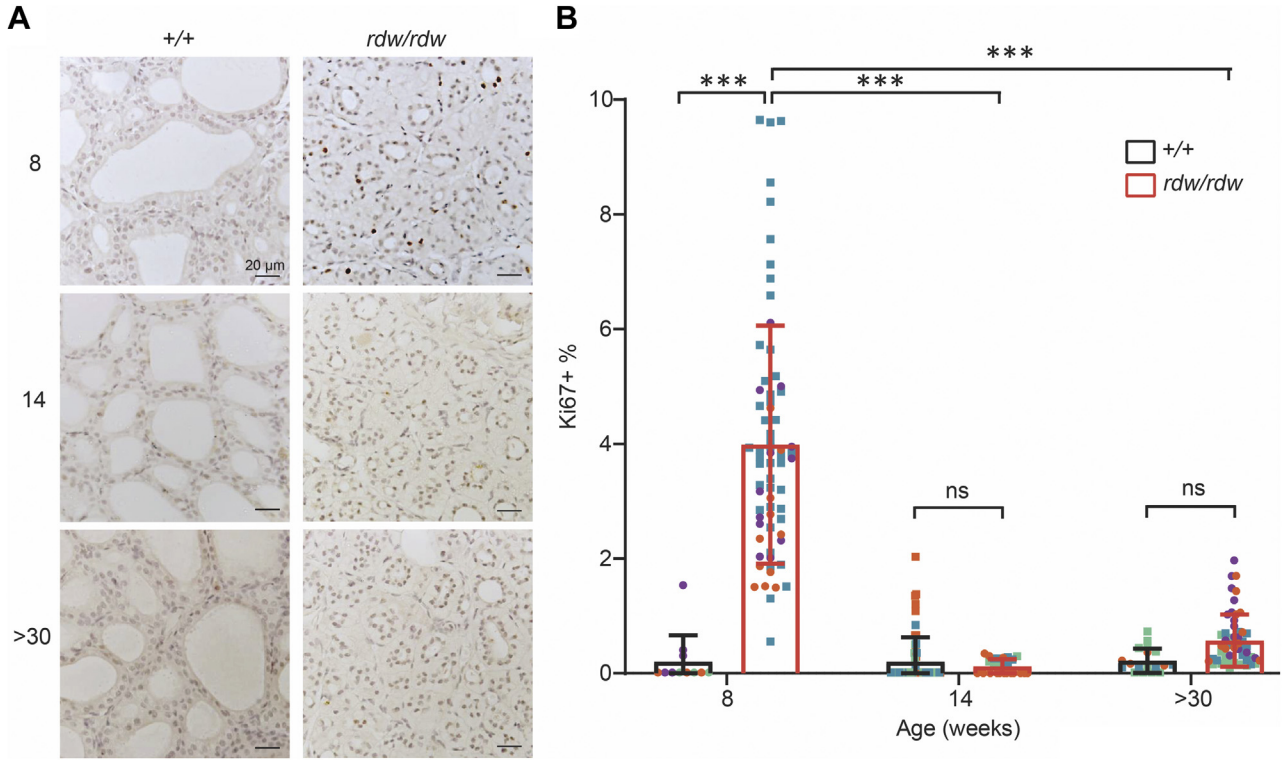

Figure 7. Thyroid cell proliferation in WIC-*TG*$^{rdw/rdw}$ rats. *A*, Ki67 immunohistochemistry of the thyroid gland of WT and WIC-*TG*$^{rdw/rdw}$ rats at 8 weeks, 14 weeks, and over 30 weeks of age. The scale bars represent 20 µm. *B*, quantification of immunostained sections like those shown in *A*, presented as Ki67-positive nuclei in the proportion of total nuclei in the thyroids of WT WIC and WIC-*TG*$^{rdw/rdw}$ rats (n = 3–4 animals per group; each color represents a single animal; each point is an independent section; *square* = male, *circle* = female). Data are mean ± SD; ***$p < 0.001$. *TG*, thyroglobulin gene.

TSH elevation (44)—or the bioactivity of the rat TSH protein itself (45)—might be insufficient in adult rats of the WIC strain. However, when we challenged older WIC rats with chemically induced hypothyroidism, we observed exuberant thyroid cell proliferation (Fig. 8), which seems to exclude that adults of the WIC strain background are deficient in adequate TSH production or action. Second is the possibility that under conditions of chronic continuous ER stress in adult WIC-*TG*$^{rdw/rdw}$ rats, those thyrocytes that do not die may adapt by developing a state of quiescence. Precedence for such a behavior has been noted in secretory cell tumor metastases that exist in a state of "antiproliferative dormancy" (46) with a highly activated ER stress response including markedly upregulated BiP levels (47) similar to what we have observed (this report, Fig. 4*A*). Indeed, dormant/latent metastatic pancreatic ductal adenocarcinoma cells exhibit a transcriptomic signature in which the single most upregulated pathway is "ER stress response" (including CHOP, linked to stress-mediated cell death; similar to what we have seen herein [Fig. 4*B*]), and the single most downregulated pathway is "cell division" (48). Indeed, deficiency of the MYRF transcription factor has been linked precisely to the same phenotype (49). Even in nontumorous pancreatic beta cells, sustained ER stress (from genetically encoded misfolded proinsulin—a secretory protein expressed approximately as abundantly as Tg protein is in thyrocytes) or impaired ER stress response (from defective PERK; a kinase that phosphorylates eIF2α) has been linked to impaired cell proliferation (50–52). Thus, loss of thyrocyte proliferation in adult WIC-*TG*$^{rdw/rdw}$ rats may in many ways be an expected result. What is remarkable is that neither hypothyroid *TG*$^{rdw/rdw}$ mice (this report) nor *TG*$^{cog/cog}$ mice (22)—nor many human patients with biallelic *TG* mutations (14, 53)—share this growth-arrest phenotype.

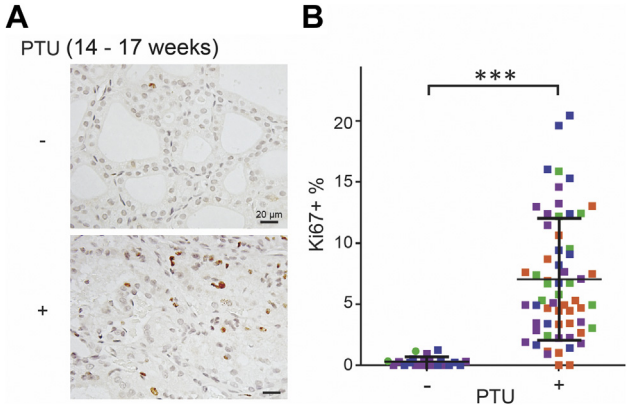

Figure 8. Thyroid cell proliferation in PTU-induced hypothyroid adult WT rats. *A*, Ki67 immunohistochemistry of the thyroid gland of control WT and PTU-treated WT rats at 17 weeks of age. Treated rats received PTU chow at 14 weeks of age for 21 days. The scale bars represent 20 µm. *B*, quantification of *A* presented as Ki67-positive nuclei in the proportion of total nuclei in the thyroids of control WT and PTU-treated WT rats (n = 3–4 animals per group; each color represents a single animal; each point is an independent section, males shown as *squares* and females as *circles*). Data are mean ± SD; ***$p < 0.001$. PTU, propylthiouracil.

Why then, would the proliferative thyroid cell response to TSH be self-limited during extended concurrent ER stress in WIC-

$TG^{rdw/rdw}$ rats? While more work is still needed to determine the difference(s) in thyroid cell proliferation in adult WIC-$TG^{rdw/rdw}$ rats *versus* $TG^{rdw/rdw}$ mice, we wonder about strain-specific differences in the abundance and response of stem/progenitor cells that may influence the long-term replicative/regenerative capacity of the thyroid gland in different vertebrates (54–59) as well as the activation GLIS3 and mechanistic target of rapamycin complex 1 activity to promote the expression of various cell cycle genes in thyrocytes (60). In addition to environmental causes (such as the level of daily dietary iodide intake in patients bearing biallelic *TG* mutations), we speculate that differences in genetic background within the human population are likely to contribute importantly to the ultimate extent of tissue regeneration and replicative growth within tissues experiencing the chronic ER stress that underlies a variety of degenerative diseases. In the meantime, what emerges from our current studies is that in congenital hypothyroidism with biallelic *TG* mutation, the ultimate development and maintenance of a large goiter requires that thyroid cell proliferation must continue unabated in adulthood.

Experimental procedures

Primary antibodies

Anti-Ki67 (SP6) (catalog no.: ab16667; Abcam); monoclonal antibody anti-Tg (catalog no.: 365997, Santa Cruz; catalog no.: ab156008, Abcam); rabbit anti-Tg and rabbit anti-BiP were previously described (13, 27); rabbit anti-Ezrin (catalog no.: PA5-17518; Invitrogen); rabbit anti-p58ipk (catalog no.: 2940; Cell Signaling Technology); rabbit anti-phospho-eIF2α (Ser51) (catalog nos.: 3597 and 9721; Cell Signaling) and total eIF2α (catalog no.: 9722; Cell Signaling); mouse antitubulin (catalog no.: T5168; Sigma); and rabbit anti-PARP (catalog no.: 9542; Cell Signaling).

Animals

Six founder $TG^{+/rdw}$ mice were generated using CRISPR/Cas9: C57BL6J zygotes received injection of guide RNA (GGTGGTCAGCTGACCATTGA) and donor vector with Tg-G2298R mutation (ACCATGGAGATGGAAGGCAGTGG TGGTCAGCTGACCATTGATCGCAGCATCCTGGCTGCA GTTGGCAACTTCATCGTAGTC) targeting *TG* exon 40 (GemPharmatech). A 534-base PCR amplicon from genomic DNA (forward primer: 5′-GTATCAAGGCAGAGCCAG CAAGA-3′; reverse primer: 5′-CAGGACTCAAAGGA GATCCTTGG-3′) was sequenced to confirm a male F0 generation mouse that harbored the heterozygous TG^{rdw} mutation. This male was bred with female C57BL6J mice to yield six F1 generation mice similarly confirmed to be $TG^{+/rdw}$ heterozygotes. These were further bred with WT C57BL6J obtained from JAX. Heterozygous crosses yielded $TG^{rdw/rdw}$ homozygotes. $TG^{cog/cog}$ mice (C57BL6J) were obtained from JAX. Mice were studied at 3 months of age unless otherwise indicated. WIC-rat $TG^{rdw/+}$ heterozygotes were obtained from the National BioResource Project in Japan (rat no: 0104) and bred to homozygosity; WT animals were littermates in the same strain background. For PTU treatment, 14-week-old WT rats were fed with low-iodide chow containing 0.15% PTU (Envigo; catalog no.: TD.95125) for 21 days. All animal experiments performed were approved by the University of Michigan Institutional Animal Care and Use Committee. Both male and female animals were used (in figures, males are represented with *squares* and females with *circles*).

Western blotting

Mouse thyroid glands were mechanically homogenized either in nondenaturing lysis buffer (20 mM Tris–HCl, pH 8, 137 mM NaCl, 1% NP-40, and 2 mM EDTA) or in radioimmunoprecipitation assay buffer (25 mM Tris–HCl, pH 7.6, 150 mM NaCl, 1% NP-40, 1% sodium deoxycholate, and 0.1% SDS; Thermo Fisher Scientific). Protease and phosphatase inhibitor cocktails (Thermo Fisher Scientific) were added to cell lysis buffer. Protein concentration was measured by bicinchoninic acid yassay (Thermo Fisher Scientific). Gel sample buffer either omitted (Fig. 1*B*) or included SDS and boiling (Fig. 1*C*) and then were resolved by 3 to 8% PAGE in the absence (Fig. 1*B*) or the presence of SDS (Fig. 1*C*). For Figures 1*D* and 4*A*, lysates were boiled in SDS-gel sample buffer plus 50 mM DTT and were then resolved by SDS—straight 4.5% or gradient 4 to 12% PAGE. Proteins were electrotransferred to nitrocellulose membranes, blocked with 5% milk, immunoblotted with the indicated antibodies and appropriate horseradish peroxidase–conjugated secondary antibody, and visualized by enhanced chemiluminescence. Endoglycosidase H digestion was performed as previously described (21).

Histology and immunostaining of thyroid sections

Thyroids from mice and rats were dissected, immersion fixed with 10% formalin, paraffin embedded, sectioned, and stained with hematoxylin–eosin (Vector). For immunofluorescence, thyroid sections (6 μm) were deparaffinized in CitriSolv, followed by antigen retrieval in citrate buffer (12.3 mM, pH 6), and blocked in 1.5% normal goat serum for 30 min at room temperature before incubation with primary antibodies overnight at 4 °C. After washing, the sections were then incubated with Alexa Fluor–conjugated secondary antibodies (Thermo Fisher Scientific) for 1 h at room temperature. Sections were counterstained with Prolong-Gold and DAPI (Invitrogen) and imaged with a Nikon A1 confocal microscope. For immunohistochemistry, anti-Ki67 staining was performed as previously described (21). Images were obtained in a Leica DMI-3000B microscope (40× objective). Analysis and quantification (Ki67-positive nuclei as a proportion of total nuclei) were performed by observers blinded to the genotypes and groups.

Serum hormone measurement

Serum total T_4, total T_3, and TSH concentrations were measured using radioimmunoassays as previously described (61, 62).

PCR

Total RNA isolation from the mouse thyroid glands was performed using RNeasy Plus kit (Qiagen), followed by reverse

transcription using the High-Capacity cDNA Reverse Transcription Kit (Thermo Fisher Scientific). For real-time PCR, PowerUp SYBR Green PCR Master Mix (Applied Biosystems) was used on a StepOnePlus PCR system (Thermo Fisher Scientific). CHOP and Tg mRNA levels were normalized to 18S RNA; primers are as follows: CHOP (forward: 5′-CCTGAGGAGAGAGTGTTCCAG-3′, reverse: 5′-GACACCGTCTCCAAGGTGAA-3′); Tg (forward: 5′-TGATCTGATCCACAACTACAACAG-3′, reverse: 5′-ATTCCAGTCCTGTCTCAGCC-3′); and 18S (forward: 5′-GGCGTCCCCCAACTTCTTA-3′, reverse: 5′-GGGCATCACAGACCTGTTATTC-3′).

TUNEL labeling

The *In Situ* Cell Death Detection Kit, Fluorescein (Roche) was used for TUNEL staining. Sections were counterstained and mounted with Prolong-Gold and DAPI. Fluorescence images were captured in a Nikon A1 confocal microscope. Quantification of TUNEL-positive nuclei in the proportion of total nuclei was performed using Imaris software (version 7.7.2; Imaris).

Thyroid gland size measurement

The areas of the thyroid glands were measured from photographic imaging at the time of dissection with an embedded millimeter rule included in each image, as previously described (21). Thyroid images for 11-month-old mice and older are shown in Fig. S4. Thyroid sizes were quantified as a fraction of body weight of each animal.

Statistics

Two-way ANOVA with Tukey's comparison sample test was used for comparison of two factors (*e.g.*, genotype plus age) and applied for statistical analysis of serum hormones, body weight, and rat thyroid Ki67 immunostaining. Unpaired two-tailed Student's *t* test was used for direct comparison of two groups (*e.g.*, CHOP or Tg mRNA level as well as TUNEL staining). One-way ANOVA followed by Tukey's multiple comparison test was used for multigroup comparison of a single factor (*e.g.*, effect of mouse genotype on thyroid Ki67 immunostaining). All statistical analyses were calculated with GraphPad Prism (GraphPad Software, Inc). All data were expressed as mean ± SD. Thyroid size measurements as a function of age were plotted by simple linear regression. Differences of $p < 0.05$ were considered significant.

Data availability

All data are contained within the article, with primary data available upon request (Dr Peter Arvan, University of Michigan, email: parvan@umich.edu).

Supporting information—This article contains supporting information.

Acknowledgments—We acknowledge the technical support of Ms Inis Isak and the Undergraduate Research Opportunity Program.

Author contributions—P. A. conceptualization; X. Z., B. M., C. Y., and X.-H. L. methodology; X. Z., B. M., C. Y., and X.-H. L. validation; X. Z., B. M., H. Z., D. L., S. R., and P. A. formal analysis; X. Z. and P. A. writing–original draft; X. Z., B. M., C. Y., H. Z., D. L., X.-H. L., S. R., M. L., and P. A. writing–review & editing; X. Z., B. M., H. Z., D. L., S. R., and P. A. visualization; P. A., S. R., and M. L. supervision; P. A., S. R., and M. L. funding acquisition.

Funding and additional information—This work was supported by the National Institutes of Health (grant no.: R01 DK132017) and from the University of Michigan Protein Folding Diseases Initiative (to P. A.) and R01 DK15070 (to S. R.). The content is solely the responsibility of the authors and does not necessarily represent the official views of the National Institutes of Health.

Conflict of interest—The authors declare that they have no conflicts of interest with the contents of this article.

Abbreviations—The abbreviations used are: BiP, immunoglobulin heavy-chain binding protein; Cas9, CRISPR-associated protein 9; CHOP, CCAAT/enhancer-binding protein homologous protein; DAPI, 4′,6-diamidino-2-phenylindole; eIF2α, eukaryotic initiation factor 2α; ER, endoplasmic reticulum; PARP, poly(ADP-ribose) polymerase; PTU, propylthiouracil; Tg, thyroglobulin protein; *TG*, thyroglobulin gene; TSH, thyroid stimulating hormone.

References

1. Brix, K., Qatato, M., Szumska, J., Venugopalan, V., and Rehders, M. (2019) "Thyroglobulin storage, processing and degradation for thyroid hormone liberation". In: Luster, M., Duntas, L. H., Wartofsky, L., eds. *The Thyroid and its Diseases: A Comprehensive Guide for the Clinician*, Springer International Publishing, Cham: 25–48
2. Holzer, G., Morishita, Y., Fini, J. B., Lorin, T., Gillet, B., Hughes, S., *et al.* (2016) Thyroglobulin represents a novel molecular architecture of vertebrates. *J. Biol. Chem.* **291**, 16553–16566
3. Di Jeso, B., and Arvan, P. (2016) Thyroglobulin from molecular and cellular biology to clinical endocrinology. *Endocr. Rev.* **37**, 2–36
4. Carvalho, D. P., and Dupuy, C. (2017) Thyroid hormone biosynthesis and release. *Mol. Cell Endocrinol.* **458**, 6–15
5. Dunn, J. T., and Dunn, A. D. (1999) The importance of thyroglobulin structure for thyroid hormone biosynthesis. *Biochimie* **81**, 505–509
6. Lamas, L., Dorris, M. L., and Taurog, A. (1972) Evidence for a catalytic role for thyroid peroxidase in the conversion of diiodotyrosine to thyroxine. *Endocrinology* **90**, 1417–1426
7. Lamas, L., and Taurog, A. (1977) The importance of thyroglobulin structure in thyroid peroxidase-catalyzed conversion of diiodotyrosine to thyroxine. *Endocrinology* **100**, 1129–1136
8. Coscia, F., Taler-Vercic, A., Chang, V. T., Sinn, L., O'Reilly, F. J., Izore, T., *et al.* (2020) The structure of human thyroglobulin. *Nature* **578**, 627–630
9. Pio, M. G., Siffo, S., Scheps, K. G., Molina, M. F., Adrover, E., Abelleyro, M. M., *et al.* (2021) Curating the gnomAD database: report of novel variants in the thyrogobulin gene using in silico bioinformatics algorithms. *Mol. Cell Endocrinol.* **534**, 111359
10. Citterio, C. E., Targovnik, H. M., and Arvan, P. (2019) The role of thyroglobulin in thyroid hormonogenesis. *Nat. Rev. Endocrinol.* **15**, 323–338
11. Morishita, Y., Kabil, O., Young, K. Z., Kellogg, A. P., Chang, A., and Arvan, P. (2020) Thyrocyte cell survival and adaptation to chronic endoplasmic reticulum stress due to misfolded thyroglobulin. *J. Biol. Chem.* **295**, 6876–6887
12. Kim, P. S., Hossain, S. A., Park, Y. N., Lee, I., Yoo, S. E., and Arvan, P. (1998) A single amino acid change in the acetylcholinesterase-like domain of thyroglobulin causes congenital goiter with hypothyroidism in the cog/cog mouse: a model of human endoplasmic reticulum storage diseases. *Proc. Natl. Acad. Sci. U. S. A.* **95**, 9909–9913

13. Kim, P. S., Kwon, O.-Y., and Arvan, P. (1996) An endoplasmic reticulum storage disease causing congenital goiter with hypothyroidism. *J. Cell Biol.* **133**, 517–527
14. Medeiros-Neto, G., Kim, P. S., Yoo, S. E., Vono, J., Targovnik, H., Camargo, R., *et al.* (1996) Congenital hypothyroid goiter with deficient thyroglobulin. Identification of an endoplasmic reticulum storage disease (ERSD) with induction of molecular chaperones. *J. Clin. Invest.* **98**, 2838–2844
15. Baryshev, M., Sargsyan, E., Wallin, G., Lejnieks, A., Furudate, S., Hishinuma, A., *et al.* (2004) Unfolded protein response is involved in the pathology of human congenital hypothyroid goiter and rat non-goitrous congenital hypothyroidism. *J. Mol. Endocrinol.* **32**, 903–920
16. Marine, D. (1924) Etiology Prev. *Simple Goiter Med.* **3**, 453–479
17. Bychkov, A. (2018) Epithelial hyperplasia is responsible for the compensatory enlargement of remaining thyroid lobe after thyroidectomy. *Eur. Arch. Otorhinolaryngol.* **275**, 2417–2419
18. Maenhaut, C., Christophe, D., Vassart, G., Dumont, J., Roger, P. P., and Opitz, R. (2000–2015) Ontogeny, anatomy, metabolism and physiology of the thyroid. In: Feingold, K. R., Anawalt, B., Boyce, A., Chrousos, G., Dungan, K., Grossman, A., *et al.* eds. *Endotext*, MDText.com, Inc, South Dartmouth (MA)
19. Oberlin, O., Plantin-Carrenard, E., Rigal, O., and Wilkinson, C. (2006) Goitre and iodine deficiency in Afghanistan: a case-control study. *Br. J. Nutr.* **95**, 196–203
20. Pisarev, M. A., DeGroot, L. J., and Wilber, J. F. (1970) Cyclic-AMP production of goiter. *Endocrinology* **87**, 339–342
21. Zhang, X., Kellogg, A. P., Citterio, C. E., Zhang, H., Larkin, D., Morishita, Y., *et al.* (2021) Thyroid hormone synthesis continues despite biallelic thyroglobulin mutation with cell death. *JCI insight* **6**, e148496
22. Adkison, L. R., Taylor, S., and Beamer, W. G. (1990) Mutant gene-induced disorders of structure, function and thyroglobulin synthesis in congenital goitre (cog/cog) in mice. *J. Endocrinol.* **126**, 51–58
23. Umezu, M., Kagabu, S., Jiang, J., and Sato, E. (1998) Evaluation and characterization of congenital hypothyroidism in rdw dwarf rats. *Lab. Anim. Sci.* **48**, 496–501
24. Menon, S., Lee, J., Abplanalp, W. A., Yoo, S. E., Agui, T., Furudate, S., *et al.* (2007) Oxidoreductase interactions include a role for ERp72 engagement with mutant thyroglobulin from the *rdw/rdw* rat dwarf. *J. Biol. Chem.* **282**, 6183–6191
25. Vono-Toniolo, J., Rivolta, C. M., Targovnik, H. M., Medeiros-Neto, G., and Kopp, P. (2005) Naturally occurring mutations in the thyroglobulin gene. *Thyroid* **15**, 1021–1033
26. Gallagher, S. R. (2018) One-dimensional electrophoresis using non-denaturing conditions. *Curr. Protoc. Protein Sci.* **94**, e73
27. Kim, P. S., and Arvan, P. (1991) Folding and assembly of newly synthesized thyroglobulin occurs in a pre-Golgi compartment. *J. Biol. Chem.* **266**, 12412–12418
28. Kim, P., Bole, D., and Arvan, P. (1992) Transient aggregation of nascent thyroglobulin in the endoplasmic reticulum: relationship to the molecular chaperone, BiP. *J. Cell Biol.* **118**, 541–549
29. Kim, K., Kopylov, M., Bobe, D., Kelley, K., Eng, E. T., Arvan, P., *et al.* (2021) The structure of natively iodinated bovine thyroglobulin. *Acta Crystallogr. D Struct. Biol.* **77**, 1451–1459
30. Lee, J., Di Jeso, B., and Arvan, P. (2011) Maturation of thyroglobulin protein region I. *J. Biol. Chem.* **286**, 33045–33052
31. Fogelfeld, L., Harel, G., Beamer, W. G., and Schneider, A. B. (1992) Low-molecular-weight iodoproteins in the congenital goiters of cog/cog mice. *Thyroid* **2**, 329–335
32. Wang, Y., Shimizu, H., Xiang, Y.-Y., Sugihara, J., Lu, W.-Y., Liao, X.-H., *et al.* (2021) XB130 deficiency causes congenital hypothyroidism in mice due to disorganized apical membrane structure and function of thyrocytes. *Thyroid* **31**, 1650–1661
33. Ulianich, L., Mirra, P., Garbi, C., Cali, G., Conza, D., Treglia, A. S., *et al.* (2020) The pervasive effects of ER stress on a typical endocrine cell: dedifferentiation, mesenchymal shift and antioxidant response in the thyrocyte. *Front. Endocrinol.* **11**, 588685
34. Hollien, J., and Weissman, J. S. (2006) Decay of endoplasmic reticulum-localized mRNAs during the unfolded protein responseJulie Hollien 1, Jonathan S Weissman. *Science* **313**, 104–107
35. Lee, A. H., Heidtman, K., Hotamisligil, G. S., and Glimcher, L. H. (2011) Dual and opposing roles of the unfolded protein response regulated by IRE1alpha and XBP1 in proinsulin processing and insulin secretion. *Proc. Natl. Acad. Sci. U. S. A.* **108**, 8885–8890
36. Coelho, D. S., and Domingos, P. M. (2014) Physiological roles of regulated Ire1 dependent decay. *Front. Genet.* **5**, 76
37. Furudate, S., Ono, M., Shibayama, K., Ohyama, Y., Kuwada, M., Kimura, T., *et al.* (2005) Rescue from dwarfism by thyroid function compensation in rdw rats. *Exp. Anim.* **54**, 455–460
38. Sakai, Y., Yamashina, S., and Furudate, S. I. (2000) Missing secretory granules, dilated endoplasmic reticulum, and nuclear dislocation in the thyroid gland of rdw rats with hereditary dwarfism. *Anat. Rec.* **259**, 60–66
39. Shimokawa, N., Yousefi, B., Morioka, S., Yamaguchi, S., Ohsawa, A., Hayashi, H., *et al.* (2014) Altered cerebellum development and dopamine distribution in a rat genetic model with congenital hypothyroidism. *J. Neuroendocrinol.* **26**, 164–175
40. Sano, R., and Reed, J. C. (2013) ER stress-induced cell death mechanisms. *Biochim. Biophys. Acta* **1833**, 3460–3470
41. Almanza, A., Carlesso, A., Chintha, C., Creedican, S., Doultsinos, D., Leuzzi, B., *et al.* (2019) Endoplasmic reticulum stress signalling - from basic mechanisms to clinical applications. *FEBS J.* **286**, 241–278
42. Lam, M., Marsters, S. A., Ashkenazi, A., and Walter, P. (2020) Misfolded proteins bind and activate death receptor 5 to trigger apoptosis during unresolved endoplasmic reticulum stress. *Elife* **9**, e52291
43. Morishita, Y., Kellogg, A. P., Larkin, D., Chen, W., Vadrevu, S., Satin, L., *et al.* (2021) Cell death-associated lipid droplet protein CIDE-A is a noncanonical marker of endoplasmic reticulum stress. *JCI insight* **6**, e143980
44. Li, A. A., Makris, S. L., Marty, M. S., Strauss, V., Gilbert, M. E., Blacker, A., *et al.* (2019) Practical considerations for developmental thyroid toxicity assessments: what's working, what's not, and how can we do better? *Regul. Toxicol. Pharmacol.* **106**, 111–136
45. Menezes-Ferreira, M. M., Petrick, P. A., and Weintraub, B. D. (1986) Regulation of thyrotropin (TSH) bioactivity by TSH-releasing hormone and thyroid hormone. *Endocrinology* **118**, 2125–2130
46. Cubillos-Ruiz, J. R., Bettigole, S. E., and Glimcher, L. H. (2017) Tumorigenic and immunosuppressive effects of endoplasmic reticulum stress in cancer. *Cell* **168**, 692–706
47. Bartkowiak, K., Kwiatkowski, M., Buck, F., Gorges, T. M., Nilse, L., Assmann, V., *et al.* (2015) Disseminated tumor cells persist in the bone marrow of breast cancer patients through sustained activation of the unfolded protein response. *Cancer Res.* **75**, 5367–5377
48. Pommier, A., Anaparthy, N., Memos, N., Kelley, Z. L., Gouronnec, A., Yan, R., *et al.* (2018) Unresolved endoplasmic reticulum stress engenders immune-resistant, latent pancreatic cancer metastases. *Science* **360**, eaao4908
49. Milan, M., Balestrieri, C., Alfarano, G., Polletti, S., Prosperini, E., Nicoli, P., *et al.* (2020) Pancreatic cancer cells require the transcription factor MYRF to maintain ER homeostasis. *Dev. Cell* **55**, 398–412.e397
50. Riahi, Y., Israeli, T., Yeroslaviz, R., Chimenez, S., Avrahami, D., Stolovich-Rain, M., *et al.* (2018) Inhibition of mTORC1 by ER stress impairs neonatal beta-cell expansion and predisposes to diabetes in the Akita mouse. *Elife* **7**, 1–25
51. Zhang, W., Feng, D., Li, Y., Iida, K., McGrath, B., and Cavener, D. R. (2006) PERK EIF2AK3 control of pancreatic beta cell differentiation and proliferation is required for postnatal glucose homeostasis. *Cell Metab.* **4**, 491–497
52. Feng, D., Wei, J., Gupta, S., McGrath, B. C., and Cavener, D. R. (2009) Acute ablation of PERK results in ER dysfunctions followed by reduced insulin secretion and cell proliferation. *BMC Cell Biol.* **10**, 61
53. Siffo, S., Adrover, E., Citterio, C. E., Miras, M. B., Balbi, V. A., Chiesa, A., *et al.* (2018) Molecular analysis of thyroglobulin mutations found in patients with goiter and hypothyroidism. *Mol. Cell Endocrinol.* **473**, 1–16

54. Hoshi, N., Kusakabe, T., Taylor, B. J., and Kimura, S. (2007) Side population cells in the mouse thyroid exhibit stem/progenitor cell-like characteristics. *Endocrinology* **148**, 4251–4258
55. Lan, L., Cui, D., Nowka, K., and Derwahl, M. (2007) Stem cells derived from goiters in adults form spheres in response to intense growth stimulation and require thyrotropin for differentiation into thyrocytes. *J. Clin. Endocrinol. Metab.* **92**, 3681–3688
56. Dumont, J. E., Lamy, F., Roger, P., and Maenhaut, C. (1992) Physiological and pathological regulation of thyroid cell proliferation and differentiation by thyrotropin and other factors. *Physiol. Rev.* **72**, 667–697
57. Ma, R., Morshed, S. A., Latif, R., and Davies, T. F. (2021) A stem cell surge during thyroid regeneration. *Front. Endocrinol. (Lausanne)* **11**, 606269
58. Kimura, S. (2014) Thyroid regeneration: how stem cells play a role? *Front. Endocrinol. (Lausanne)* **5**, 55
59. Finkielstain, G. P., Forcinito, P., Lui, J. C., Barnes, K. M., Marino, R., Makaroun, S., *et al.* (2009) An extensive genetic program occurring during postnatal growth in multiple tissues. *Endocrinology* **150**, 1791–1800
60. Kang, H. S., Kumar, D., Liao, G., Lichti-Kaiser, K., Gerrish, K., Liao, X.-H., *et al.* (2017) GLIS3 is indispensable for TSH/TSHR-dependent thyroid hormone biosynthesis and follicular cell proliferation. *J. Clin. Invest.* **127**, 4326–4337
61. Dumitrescu, A. M., Liao, X. H., Weiss, R. E., Millen, K., and Refetoff, S. (2006) Tissue-specific thyroid hormone deprivation and excess in monocarboxylate transporter (mct) 8-deficient mice. *Endocrinology* **147**, 4036–4043
62. Pohlenz, J., Maqueem, A., Cua, K., Weiss, R. E., Van Sande, J., and Refetoff, S. (1999) Improved radioimmunoassay for measurement of mouse thyrotropin in serum: strain differences in thyrotropin concentration and thyrotroph sensitivity to thyroid hormone. *Thyroid* **9**, 1265–1271